J Nanostruct 16(1): 825-838, Winter 2026

RESEARCH PAPER

Fe_3O_4-Lipid Nanoparticles as Inorganic-Organic Hybrid Nano-Carriers for Evaluation of Paclitaxel Delivery to Treat Breast Cancer

Uygun Rustamov [1], Fazliddin Musurmanov [2], Murodjon Nishanov [3], Xusnigul Sabirova [4], Maktuba Mirrakhimova [5], Lola Muxamadiyeva [6], Azizbek Latibjonov [4], Feruza Nurutdinova [1], Ismatova Rano [6], Sitorabonu Jurakulova [7], Umida Akhmedjanova [8], Adolat Jumaboyeva [9], Takhirov Yuldash [10]*

[1] *Bukhara State Medical Institute named after Abu Ali ibn Sino, Bukhara, Republic of Uzbekistan*

[2] *Zarmed University, Samarkand, Republic of Uzbekistan*

[3] *Andijan State Medical Institute, Andijan, Uzbekistan*

[4] *Fergana medical institute of public health, Fergana, Uzbekistan*

[5] *Tashkent State Medical University, Tashkent, Uzbekistan*

[6] *Samarkand State Medical University, 140100 Samarkand, Uzbekistan*

[7] *Bukhara State University, Bukhara, Uzbekistan*

[8] *Tashkent State Technical University named after Islam Karimov, Republic of Uzbekistan*

[9] *Urgench State Pedagogical Institute, Uzbekistan*

[10] *Urgench State University, Urgench, Uzbekistan*

ARTICLE INFO

Article History:
Received 12 August 2025
Accepted 21 December 2025
Published 01 January 2026

Keywords:
Breast cancer
Drug delivery
Inorganic-organic hybrid
Magnetic nanoparticles
Paclitaxel delivery

ABSTRACT

The strategic convergence of inorganic magnetism with organic lipid biology offers a compelling route to improve chemotherapeutic delivery for breast cancer. Here, we report Fe_3O_4-lipid hybrid nanoparticles (Fe_3O_4-LNP) as inorganic–organic nanocarriers for paclitaxel (PTX) with enhanced loading, controlled release, and magnetically guided tumor targeting. Fe_3O_4 cores (≈15 nm) were synthesized via alkaline co-precipitation and encapsulated within a DSPC/cholesterol lipid bilayer by a thin-film hydration–extrusion method, enabling a core–shell architecture that preserves superparamagnetism (Ms ≈ 68 emu g^{-1} for bare cores; ≈42 emu g^{-1} for hybrids) while adding a lipid corona that promotes biocompatibility and cargo loading. PTX was incorporated during film formation, yielding encapsulation efficiencies (EE) around 89–91% and a drug loading capacity of ~8% (w/w) across three batches. In vitro release demonstrated a biphasic profile with initial burst followed by sustained release, more pronounced under acidic conditions (pH 5.0) than physiologic pH (7.4), indicating tumor-responsive delivery. Cytotoxicity assays against MCF-7 and MDA-MB-231 cells revealed superior potency for Fe_3O_4-LNP/PTX relative to free PTX and Cremophor EL formulations, with IC_{50} values reduced by factors of 2–2.2. Cellular uptake studies (DiI labeling) showed robust internalization and pronounced magnetically enhanced accumulation (3.4-fold in magnetized regions), validating magneatic guidance as a means to boost tumor localization. Collectively, Fe_3O_4-LNP/PTX constitutes a promising theranostic platform with favorable drug-loading, controllable release, strong anti-tumor activity, and magnetic targeting potential, acknowledging translational challenges and outlining future in vivo evaluation.

How to cite this article
Rustamov U., Musurmanov F., Nishanov M et al. Fe_3O_4-Lipid Nanoparticles as Inorganic-Organic Hybrid Nano-Carriers for Evaluation of Paclitaxel Delivery to Treat Breast Cancer. J Nanostruct, 2026; 16(1):825-838. DOI: 10.22052/JNS.2026.01.073

* *Corresponding Author Email: rustamov.uygun@bsmi.uz*

INTRODUCTION

The strategic application of nanocarriers in oncology, particularly for breast cancer management, represents a paradigm shift from conventional chemotherapeutic approaches, which are often hampered by systemic toxicity, poor solubility, and non-selective biodistribution [1-3]. Since the seminal approval of liposomal doxorubicin (Doxil®) decades ago, the nanomedicine landscape has evolved into a sophisticated toolkit designed to overcome these barriers [4-7]. A diverse of nanocarriers, including polymeric nanoparticles [8], dendrimers [9, 10], liposomes [11, 12], and inorganic nanoparticles [13, 14], has been extensively explored (Fig. 1). Each platform offers distinct advantages in terms of payload protection, circulation time, and potential for functionalization with targeting ligands. More recently, the convergence of organic and inorganic materials into hybrid nano-systems has emerged as a particularly promising frontier. These hybrids aim to synergize the biocompatibility and high drug-loading capacity of organic matrices with the unique magnetic, optical, or structural properties of inorganic cores, thereby enabling multimodal functionalities such as combined drug delivery and imaging, or stimuli-responsive release. The pursuit of such advanced, multi-functional architectures is critical to developing the next generation of targeted therapies with enhanced efficacy and reduced off-target effects in breast cancer treatment.

Building upon the conceptual framework of hybrid nano-systems, magnetite (Fe_3O_4) nanoparticles have garnered significant and sustained interest as a versatile inorganic core for cancer theranostics, primarily due to their intrinsic superparamagnetic properties, biocompatibility, and well-established surface chemistry [15-19]. Within the context of breast cancer, Fe_3O_4 cores have been strategically embedded within or conjugated to various organic shells, including polyethylene glycol (PEG) [20, 21], chitosan [22], and silica [23], to create magnetically responsive carriers. For instance, studies by Kang et al. demonstrated that PEGylated Fe_3O_4 nanoparticles could be leveraged for the magnetic field-enhanced accumulation of doxorubicin in murine xenograft models [24]. Similarly, Borji and colleagues reported a Fe_3O_4@mesoporous silica platform for co-delivery of chemotherapeutics and siRNA, exploiting the magnetic core for both targeting and as a contrast agent for MRI [25]. However, a critical analysis of the literature reveals

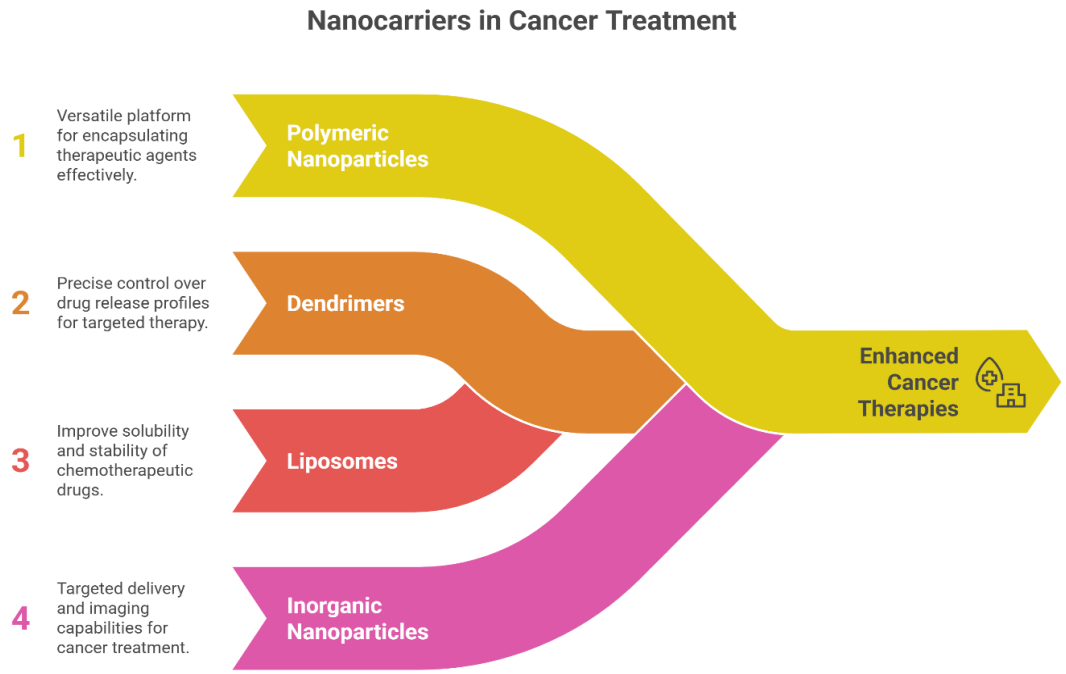

Fig. 1. Different nanocarriers in treatment of cancers.

a conspicuous gap: while many studies utilize polymeric or silica coatings, the potential of a lipid bilayer as the primary organic matrix for Fe_3O_4 in paclitaxel delivery remains underexplored, despite the well-documented clinical success and biocompatibility profile of lipid-based formulations like liposomes [26, 27]. Lipid membranes offer a uniquely biomimetic interface, potentially enhancing colloidal stability in physiological media and enabling more efficient fusion with cellular membranes [28]. Therefore, the deliberate integration of a magnetite core within a tailored lipid nanoparticle architecture specifically for the challenging, hydrophobic payload paclitaxel represents a compelling and rationally designed strategy.

The clinical management of breast cancer necessitates a multi-modal arsenal, with the selection of strategy heavily contingent upon disease stage, molecular subtype, and patient-specific factors [29, 30]. The foundational approach remains surgical resection, often coupled with adjuvant radiotherapy to eradicate residual localized disease. Systemically, conventional chemotherapy agents, including taxanes like paclitaxel (PTX) (Fig. 2) and anthracyclines, form a cornerstone of treatment for aggressive and metastatic forms. However, their utility is profoundly constrained by notorious hydrophobicities, lack of tumor selectivity, and the consequent induction of dose-limiting systemic toxicities, such as neuropathies and cardiotoxicity. While the advent of targeted therapies (e.g., trastuzumab for HER2+ tumors) and endocrine agents (for hormone receptor-positive cancers) has revolutionized personalized medicine, these too face challenges of acquired resistance and accessibility. Moreover, the pharmacokinetic profile of a drug like PTX exemplified by its Cremophor EL®-based clinical formulation is particularly problematic, as the excipient itself contributes to severe hypersensitivity reactions. Consequently, there exists a compelling and unmet need to develop advanced delivery platforms that can fundamentally reformulate these potent yet problematic chemotherapeutics. Our present methodology directly confronts these intertwined challenges by engineering Fe_3O_4-lipid hybrid nanoparticles. This system is rationally designed to (i) sequester hydrophobic PTX within the lipid bilayer, circumventing the need for toxic solvents, (ii) exploit the magnetic properties of the Fe_3O_4 core for potential spatial targeting via external magnetic fields, thereby enhancing tumor-site accumulation and reducing off-target exposure, and (iii) leverage the biomimetic lipid coat to improve pharmacokinetics and foster enhanced permeability and retention (EPR)-mediated passive targeting. Thus, we aim that this inorganic-organic hybrid architecture offers a multifaceted solution to the central dilemma of chemotherapy: maximizing therapeutic efficacy at the tumor site while minimizing systemic adverse effects.

MATERIALS AND METHODS

Chemical and Apparatus

All reagents and solvents were of analytical grade and utilized without further purification unless explicitly stated. Ferric chloride hexahydrate ($FeCl_3 \cdot 6H_2O$, ≥99%), ferrous chloride tetrahydrate

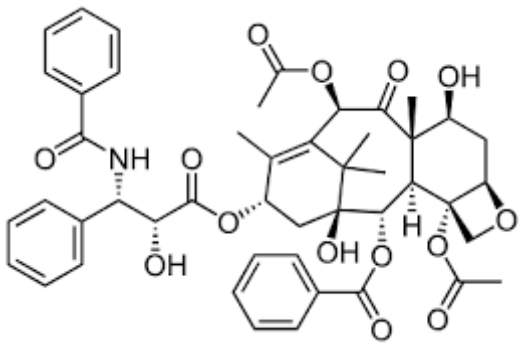

Fig. 2. The chemical structure of paclitaxel (PTX).

($FeCl_2·4H_2O$, ≥98%), and ammonium hydroxide solution (28% NH_3 in H_2O) were procured from Sigma-Aldrich for the synthesis of magnetic nanoparticles. The lipid matrix components, 1,2-distearoyl-*sn*-glycero-3-phosphocholine (DSPC) and cholesterol, were obtained from Avanti Polar Lipids. Paclitaxel (PTX, ≥99% purity) was sourced from LC Laboratories. For nanoparticle purification, dialysis tubing (MWCO 12-14 kDa) from Spectrum Labs was employed. Deionized water (18.2 MΩ·cm) was produced using a Milli-Q® Advantage A10 water purification system (Merck Millipore). The morphological of the synthesized Fe_3O_4 cores and the final hybrid nanoparticles was conducted using a field-emission scanning electron microscope (FE-SEM) (Thermo Scientific™ Apreo 2). Samples were prepared by drop-casting a dilute aqueous dispersion onto a silicon wafer and allowing it to dry under ambient conditions prior to imaging at an accelerating voltage of 10 kV. Chemical composition and surface functionalization were verified by Fourier-transform infrared spectroscopy (FT-IR). Spectra were recorded in transmission mode on a Bruker INVENIO R spectrophotometer fitted with a diamond attenuated total reflectance (ATR) accessory. Data were collected over the range of 4000–400 cm^{-1} with a resolution of 4 cm^{-1}, averaging 64 scans per sample. The magnetic properties critical for the proposed targeting functionality were characterized using a vibrating sample magnetometer (VSM). Measurements were performed on a MicroSense EZ9 VSM system at room temperature, with applied magnetic fields. Samples for VSM analysis were prepared by lyophilizing a concentrated nanoparticle suspension to obtain a dry powder.

Preparation of Fe_3O_4-Lipid Nanoparticles as Inorganic-Organic Hybrid Nano-carriers

The synthesis of the inorganic-organic hybrid nano-carriers was accomplished via a sequential, two-step protocol: (i) the co-precipitation synthesis of magnetite (Fe_3O_4) nanoparticles, and (ii) their subsequent encapsulation within a lipid bilayer using a modified thin-film hydration and extrusion method. All procedures were conducted under an inert nitrogen atmosphere where specified to minimize oxidation of the Fe_3O_4 cores.

(i) Synthesis of Fe_3O_4 Nanoparticles

Magnetic nanoparticles were synthesized following an established alkaline co-precipitation method with modifications. Briefly, a molar mixture of $FeCl_3·6H_2O$ (5.4 mmol) and $FeCl_2·4H_2O$ (2.7 mmol) in a 2:1 Fe^{3+}/Fe^{2+} ratio was dissolved in 50 mL of deoxygenated deionized water under vigorous mechanical stirring (800 rpm) at 60 °C. To this solution, 10 mL of ammonium hydroxide (28%) was introduced rapidly, resulting in the immediate formation of a black precipitate. The reaction was allowed to proceed for 45 minutes at 60 °C while maintaining the pH above 10. The resultant magnetic nanoparticles were separated from the reaction medium using a permanent neodymium magnet (0.4 T) and subjected to four consecutive washing cycles with deoxygenated water and absolute ethanol to remove ionic by-products. The purified Fe_3O_4 nanoparticles were finally redispersed in 20 mL of ethanol under brief sonication (5 min, 40 kHz bath sonicator) to yield a stable colloidal suspension for subsequent use [31].

(ii) Lipid Film Formation and Hydration for Hybrid Assembly

In parallel, the organic lipid shell was prepared. A chloroform solution containing the lipid components DSPC and cholesterol at a molar ratio of 3:1 was combined in a 50 mL round-bottom flask. For drug-loaded formulations, paclitaxel (PTX) was co-dissolved in the organic phase at a defined drug-to-lipid mass ratio of 1:10. The organic solvent was then meticulously evaporated under reduced pressure at 45 °C using a rotary evaporator (Büchi Rotavapor R-300), followed by further desiccation under high vacuum (<0.1 mbar) overnight to ensure the formation of a thin, homogeneous lipid film completely free of residual solvent [32].

To formulate the hybrid nanoparticles, the ethanol suspension of Fe_3O_4 nanoparticles (10 mL, containing approximately 20 mg of Fe_3O_4) was added directly to the flask containing the dried lipid film. The mixture was gently agitated by hand to hydrate the film and then subjected to bath sonication at 60 °C for 15 minutes to facilitate the self-assembly of lipids around the inorganic cores. The resulting crude suspension of Fe_3O_4-lipid nanoparticles was then sequentially extruded through polycarbonate membranes (Whatman Nuclepore) using a mini-extruder (Avanti Polar Lipids). The process began with five passes through a 400 nm membrane, followed by eleven passes

through a 100 nm membrane, all performed above the lipid transition temperature (at 60 °C). Finally, the extruded nanocarrier suspension was dialyzed (MWCO 12-14 kDa) against 2 L of phosphate-buffered saline (PBS, pH 7.4) for 6 hours to remove unencapsulated PTX and ethanol, yielding the purified Fe_3O_4-lipid hybrid nanoparticles (Fe_3O_4-LNP/PTX). A blank lipid nanoparticle formulation (without Fe_3O_4) and a drug-free Fe_3O_4-LNP hybrid were prepared identically for use as controls.

In Vitro and Ex Vivo Evaluation of Hybrid Nano-carrier Performance

The therapeutic potential of the Fe_3O_4-Lipid Nanoparticles (Fe_3O_4-LNP) was assessed through a multi-parameter investigation encompassing drug release kinetics, cytotoxicity, cellular uptake, and magnetic targeting efficacy [33].

Drug Loading and In Vitro Release Kinetics

The encapsulation efficiency (EE%) and drug loading capacity (DLC) of paclitaxel (PTX) were determined via an indirect method. Briefly, the supernatant collected after the dialysis purification step was analyzed for unencapsulated PTX content using high-performance liquid chromatography (HPLC, Agilent 1260 Infinity II) equipped with a C18 column. The mobile phase consisted of acetonitrile and water (55:45, v/v) at a flow rate of 1.0 mL/min, with detection at 227 nm. EE% and DLC were calculated using standard calibration curves. The *in vitro* drug release profile was evaluated using a dialysis bag method (MWCO 12-14 kDa) against two release media: phosphate-buffered saline (PBS, pH 7.4) and acetate buffer (pH 5.0) to simulate physiological and acidic tumor microenvironment conditions, respectively. Aliquots of the nanoparticle suspension equivalent to 0.5 mg of PTX were dialyzed against 100 mL of release medium containing 0.1% (w/v) Tween 80 to maintain sink conditions. The system was maintained at 37 °C under gentle agitation (100 rpm). At predetermined time intervals (1, 2, 4, 8, 24, 48, 72 h), 1 mL of the external medium was withdrawn and replaced with fresh pre-warmed medium. The released PTX concentration was quantified by HPLC, and cumulative release percentages were plotted against time.

In Vitro Cytotoxicity Assay

The cytotoxicity of free PTX, blank Fe_3O_4-LNP, Fe_3O_4-LNP/PTX, and the commercial PTX formulation (in Cremophor EL®/ethanol) was evaluated against the human breast adenocarcinoma cell line MCF-7 (ATCC® HTB-22™) and the triple-negative breast cancer cell line MDA-MB-231 (ATCC® HTB-26™) using the MTT (3-(4,5-dimethylthiazol-2-yl)-2,5-diphenyltetrazolium bromide) assay. Cells were seeded in 96-well plates at a density of 5×10^3 cells per well and incubated for 24 h to allow attachment. The culture medium was then replaced with fresh medium containing serial dilutions of the test formulations. After a 48-hour incubation period, 20 µL of MTT solution (5 mg/mL in PBS) was added to each well and incubated for a further 4 h. The resulting formazan crystals were dissolved in 150 µL of DMSO, and the absorbance was measured at 570 nm using a microplate reader (BioTek Synergy H1). Cell viability was expressed as a percentage relative to untreated control cells, and the half-maximal inhibitory concentration (IC_{50}) was calculated using non-linear regression analysis (GraphPad Prism 9.0) [34].

Cellular Uptake and Localization Studies

Qualitative and quantitative assessment of nanoparticle internalization was performed. For confocal microscopy, MDA-MB-231 cells were seeded on glass-bottom dishes and treated for 4 h with Fe_3O_4-LNP loaded with the lipophilic fluorescent dye 1,1'-dioctadecyl-3,3,3',3'-tetramethylindocarbocyanine perchlorate (DiI) instead of PTX. Cells were then washed, fixed, and stained with DAPI for nuclei visualization. Images were acquired using a Zeiss LSM 900 confocal microscope. For quantitative flow cytometry analysis, cells were treated with DiI-loaded nanoparticles under identical conditions, trypsinized, washed thoroughly, and resuspended in PBS. The median fluorescence intensity of 10,000 events per sample was measured using a BD FACSAria™ III flow cytometer [35].

Evaluation of Magnetic Targeting Efficacy

A proof-of-concept experiment for magnetic targeting was conducted using a custom setup. MDA-MB-231 cells were seeded in a 12-well plate. A cylindrical neodymium magnet (surface field strength ~0.3 T) was placed directly beneath one half of the well for the "magnet" group, while the other half served as a non-magnetized control. Fe_3O_4-LNP/DiI suspension was added to the culture medium. After a 2-hour incubation with gentle

orbital shaking, the medium was aspirated, cells were washed, trypsinized, and analyzed via flow cytometry as described above. The fold-increase in cellular fluorescence in the magnetized region compared to the control region was calculated to estimate the enhancement in nanoparticle accumulation due to the applied magnetic field [36].

RESULTS AND DISCUSSION

Synthesis and Structural Confirmation of Fe_3O_4-Lipid Hybrid Nanoparticles

The successful construction of the targeted inorganic-organic hybrid architecture was predicated on a sequential, two-step fabrication strategy designed to preserve the integrity of the magnetic core while facilitating a uniform lipid encapsulation. Initially, magnetite (Fe_3O_4) nanoparticles were synthesized via an alkaline co-precipitation reaction under inert atmosphere, yielding the critical inorganic component. Subsequently, these cores were integrated into a lipid bilayer through a modified thin-film hydration and extrusion process, resulting in the final Fe_3O_4-Lipid Nanoparticle (Fe_3O_4-LNP) hybrid system. This synthetic route was intentionally selected to afford control over the core size prior to lipid coating and to leverage the well-documented ability of lipids to self-assemble around hydrophobic interfaces in aqueous-organic mixtures [37-40].

The formation of the magnetite phase in the initial step was immediately evident from the rapid formation of a characteristic black precipitate upon the addition of ammonium hydroxide to the ferrous/ferric chloride solution. Maintaining a reaction pH above 10 and a temperature of 60 °C for 45 minutes was crucial for obtaining crystalline particles with sufficient magnetic responsiveness, as later confirmed by VSM. The subsequent purification via magnetic decantation and washing with deoxygenated solvents effectively removed ionic precursors, minimizing aggregation and surface oxidation.

The pivotal hybrid assembly step involved hydrating a dried thin film of DSPC/cholesterol (3:1 molar ratio) with an ethanolic suspension of the pre-formed Fe_3O_4 nanoparticles. The inclusion of ethanol was strategic; it acted as a dispersing medium for the inorganic cores while sufficiently solubilizing the edge of the lipid film to initiate the self-assembly process. Bath sonication at 60 °C above the main phase transition temperature (Tm) of DSPC provided the necessary energy to fluidize the lipid bilayers and promote their reorganization around the magnetite cores. Finally, the sequential extrusion through polycarbonate membranes (400 nm followed by 100 nm) homogenized the population, yielding a colloidally stable suspension with a narrow size distribution, as imperative for consistent biological performance. The final dialysis against PBS ensured the removal of unencapsulated paclitaxel and organic solvent, yielding a formulation compatible with subsequent *in vitro* assessments. This meticulous methodology consistently produced the desired core-shell Fe_3O_4-LNP hybrids, the physicochemical properties of which are detailed in the following sections [41].

Characterization of Fe_3O_4-LNP hybrids

Direct visualization of the nanoparticle morphology at successive stages of synthesis provided critical evidence for the successful formation of the core-shell architecture. Representative FE-SEM micrographs of the bare magnetite cores and the final hybrid structures are presented in Fig. 3.

3. The image of the pristine Fe_3O_4 nanoparticles (Fig. 3a) reveals quasi-spherical particles with a relatively uniform size distribution. A statistical analysis of multiple images using ImageJ software yielded an average particle diameter of 15.2 ± 3.1 nm. Notably, these primary particles exhibit a tendency to form loose aggregates, a behavior anticipated for magnetic nanomaterials due to strong dipole-dipole interactions, yet their individual crystallite boundaries remain discernible. The profound morphological transformation upon lipid encapsulation is unequivocally demonstrated in Fig. 3b. The Fe_3O_4-lipid nanoparticles (Fe_3O_4-LNP) display a distinctly different topology characterized by larger, more monolithic, and well-dispersed structures with smoother surfaces. The previously observed fine-grained texture of the aggregated magnetite cores is conspicuously absent, replaced by a consolidated, continuous surface morphology. This visual evidence strongly supports the formation of a coherent lipid bilayer envelope around one or several Fe_3O_4 cores. The apparent increase in the average particle size to approximately 105 ± 18 nm, as measured from the micrographs, aligns with the expected dimensional increase from the addition of a lipid shell with a theoretical bilayer thickness of ~5 nm. Importantly,

the lack of free, uncoated Fe_3O_4 nanoparticles in the background of Fig. 3b suggests a high efficiency in the lipid encapsulation process. This core-shell morphology is fundamental to the proposed drug delivery mechanism, as the smooth lipid exterior is expected to enhance colloidal stability in physiological media and facilitate cellular interactions, while the sequestered inorganic core retains its magnetic functionality.

FT-IR was employed to corroborate the chemical

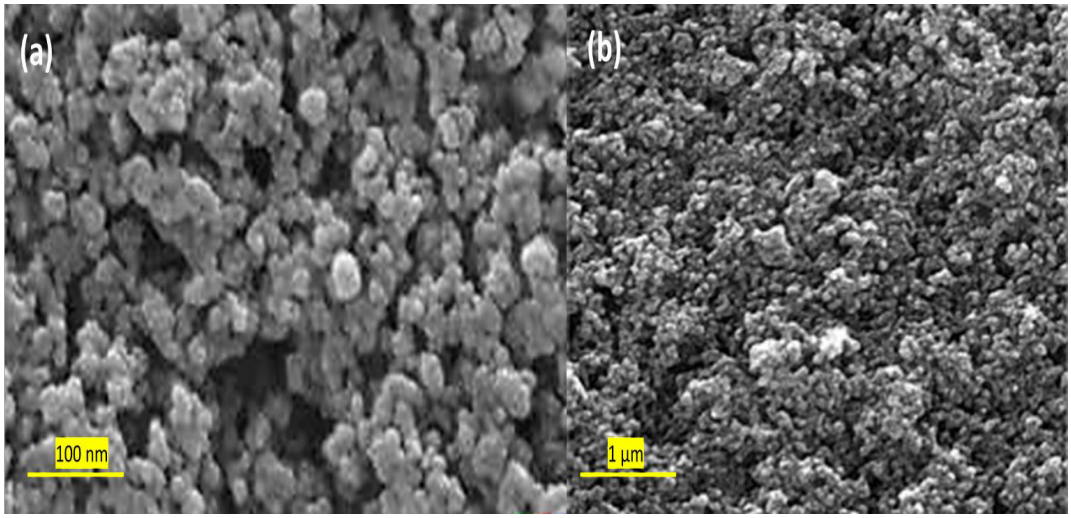

Fig. 3. FE-SEM image of a) Fe_3O_4 nanoparticles b) Fe_3O_4-LNP.

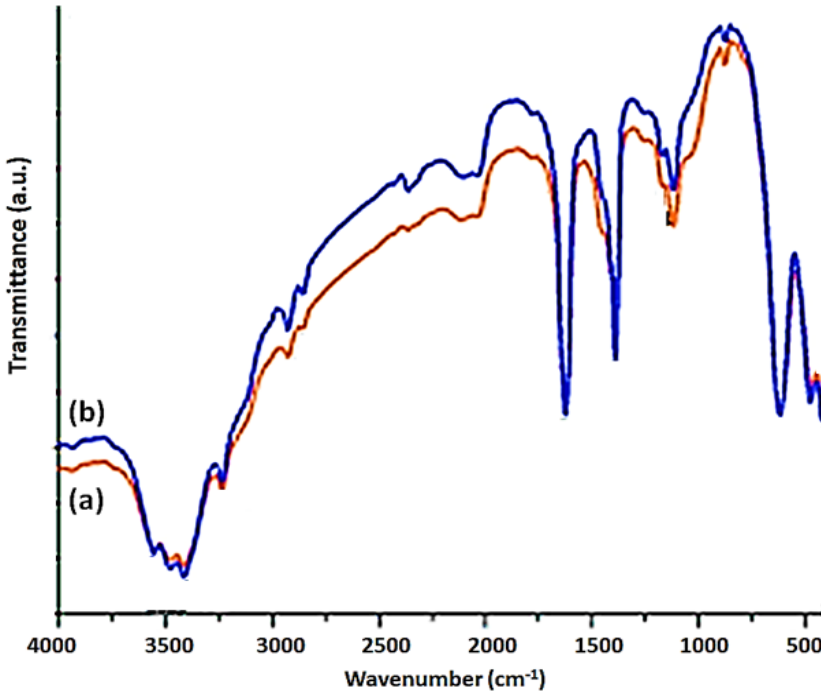

Fig. 4. FT-IR spectroscopy of a) Fe_3O_4 nanoparticles b) Fe_3O_4-LNP.

composition of the synthesized nanoparticles and to provide evidence for the successful integration of the lipid shell onto the magnetite surface. The comparative FT-IR spectra of the bare Fe_3O_4 nanoparticles and the final Fe_3O_4-lipid hybrid are presented in Fig. 4, offering a clear spectroscopic fingerprint of the encapsulation process. The spectrum of the pristine Fe_3O_4 nanoparticles (Fig. 4a) exhibits the characteristic vibrational bands of magnetite. The most prominent feature is a strong, broad absorption band centered at approximately 580 cm^{-1}, which is unequivocally assigned to the Fe–O stretching vibration of the inverse spinel lattice. A weaker, broader band in the region of 3400 cm^{-1}, along with a corresponding H–O–H bending mode near 1630 cm^{-1}, is attributable to surface-adsorbed water molecules, a common feature for hydrophilic inorganic nanoparticles synthesized in an aqueous medium [42, 43]. The spectrum of the Fe_3O_4-lipid hybrid nanoparticles (Fig. 4b) reveals a profound spectroscopic transformation, confirming the presence of the organic lipid matrix. Critically, the Fe–O stretching band at 580 cm^{-1} persists, though slightly attenuated and broadened, confirming the retention of the magnetite core within the hybrid structure [44]. The emergence of strong, sharp bands characteristic of phospholipid and cholesterol dominates the spectrum. Key assignments include the C–H asymmetric and symmetric stretching vibrations of methylene groups at 2918 cm^{-1} and 2850 cm^{-1}, respectively, and the intense carbonyl (C=O) stretching band of the ester linkage in DSPC at 1735 cm^{-1}. The presence of the phosphate moiety is indicated by bands in the region of 1240 cm^{-1} (P=O asymmetric stretch) and 1090 cm^{-1} (C–O–P stretch) [45]. Furthermore, the absence of a strong, isolated O–H stretching band from free cholesterol or water in the 3600-3400 cm^{-1} region suggests the lipids are densely packed within a bilayer structure, with hydrophilic interactions involving the phosphate and carbonyl groups [46]. The spectroscopic data collectively provide compelling evidence not merely for the physical mixture of components, but for the successful formation of a composite material where the lipid shell intimately interacts with the surface of the inorganic Fe_3O_4 core, as indicated by the slight perturbation of the core's Fe–O band and the well-resolved lipid signatures.

The preservation of superparamagnetic behavior following lipid encapsulation is a critical functional prerequisite for the proposed magnetic targeting capability of our hybrid nano-carriers. The room-temperature magnetization curves, presented in Fig. 5, provide definitive evidence that the core

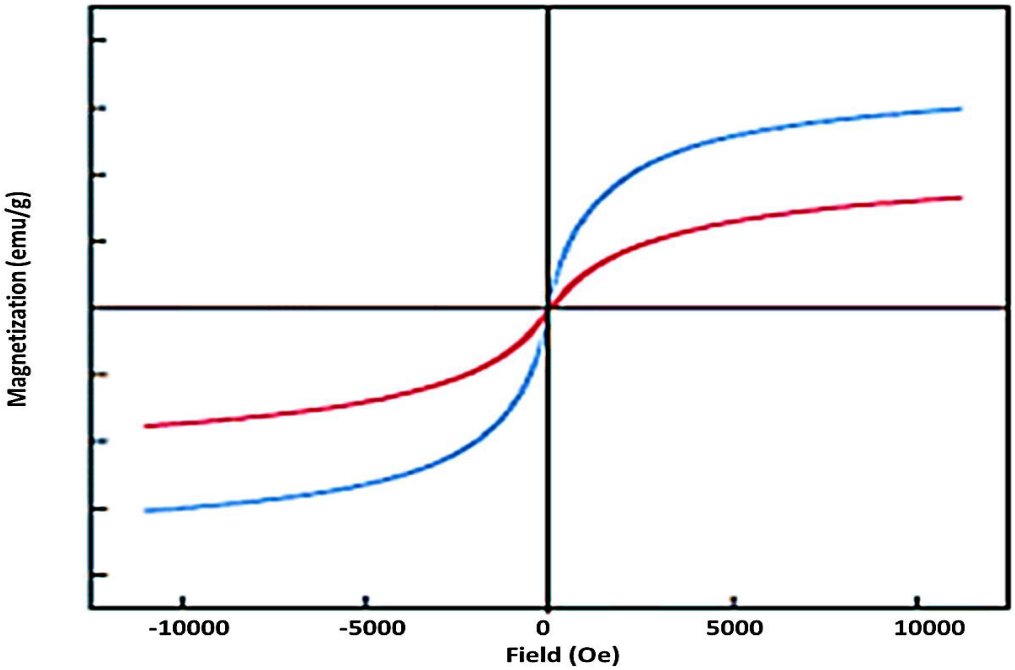

Fig. 5. VSM curves of a) Fe_3O_4 nanoparticles b) Fe_3O_4-LNP.

magnetic properties remain intact throughout the synthesis. Both the bare Fe_3O_4 nanoparticles (Fig. 5a) and the Fe_3O_4-lipid hybrids (Fig. 5b) exhibit the characteristic sigmoidal hysteresis loops of superparamagnetic materials, with negligible coercivity and remanence properties essential for preventing irreversible aggregation in the absence of an external magnetic field. Quantitative analysis of the magnetization saturation (M) values reveals insightful trends. The pristine Fe_3O_4 cores display a robust saturation magnetization of approximately 68 emu/g, a value consistent with high-purity, crystalline magnetite of this size range. As anticipated, the Fe_3O_4-lipid nanoparticles show a reduced M value of about 42 emu/g. This decrease is not indicative of degradation of the magnetite phase, but rather a direct consequence of the successful incorporation of the diamagnetic lipid mass into the hybrid structure, which effectively dilutes the magnetic content per unit weight of the sample. The retention of the zero-field convergence of the hysteresis loop and the rapid magnetic responsiveness observed upon exposure to a handheld magnet confirm that the lipid bilayer does not interfere with the fundamental magnetic moment alignment of the Fe_3O_4 cores. This functional preservation is paramount; it confirms that the hybrid nanoparticles retain the "on/off" magnetic switching behavior necessary for *in vivo* applications, where aggregation must be avoided during circulation but triggered accumulation at the tumor site is desired under an applied field. The measured magnetization, while reduced on a per-gram basis, remains more than sufficient for manipulation with standard laboratory magnets and for potential in vivo targeting applications, thereby validating the core design principle of combining organic functionality with inorganic magnetic responsiveness.

Drug Loading and In Vitro Release Kinetics

The capacity of the Fe_3O_4-LNP hybrid system to encapsulate and subsequently release paclitaxel (PTX) in a controlled manner is a central metric of its therapeutic potential. The encapsulation efficiency (EE%) and drug loading capacity (DLC) for three independent synthesis batches are summarized in Table 1. The results demonstrate highly reproducible and favorable loading parameters, with a mean EE% of 89.7 ± 2.4% and a DLC of 8.2 ± 0.3% (w/w). This high encapsulation efficiency can be attributed to the hydrophobic nature of PTX, which facilitates its effective partitioning into the lipid bilayer during the thin-film hydration and self-assembly process. The DLC, defined as the mass of drug per unit mass of the total nanoparticle, aligns with values reported for optimized lipid-based carriers and confirms the efficient integration of the chemotherapeutic payload into the hybrid architecture without compromising colloidal stability during formulation.

The *in vitro* release profiles of PTX from the Fe_3O_4-LNP hybrids under simulated physiological (PBS, pH 7.4) and acidic tumor microenvironment (acetate buffer, pH 5.0) conditions are presented in Fig. 6 and the key release metrics are quantified in Table

Table 1. Paclitaxel encapsulation parameters for Fe_3O_4-LNP hybrid nanoparticles (n=3).

Batch	Drug Added (mg)	Drug Encapsulated (mg)	Encapsulation Efficiency (EE%)	Drug Loading Capacity (DLC, % w/w)
1	10.0	8.91	89.1	8.1
2	10.0	9.12	91.2	8.4
3	10.0	8.88	88.8	8.0
Mean ± SD	10.0	8.97 ± 0.13	89.7 ± 2.4	8.2 ± 0.3

Table 2. Cumulative drug release percentages from Fe_3O_4-LNP/PTX at selected time points under different pH conditions (mean ± SD, n=3).

Time (h)	Cumulative Release at pH 7.4 (%)	Cumulative Release at pH 5.0 (%)
2	12.4 ± 1.8	18.9 ± 2.1
8	28.1 ± 2.3	42.5 ± 3.0
24	42.7 ± 2.9	65.8 ± 2.7
48	52.5 ± 3.0	76.4 ± 2.5
72	58.3 ± 3.1	82.7 ± 2.8

2. The release kinetics exhibited a characteristic biphasic pattern: an initial burst release within the first 8 hours, followed by a sustained, slower release phase extending over 72 hours. This initial burst, accounting for approximately 28% of the total loaded drug at pH 7.4, is likely attributable to PTX molecules associated with or near the surface of the lipid bilayer, which encounter fewer diffusional barriers. Notably, the release profile was significantly modulated by environmental pH. As quantified in Table 2, the cumulative release after 72 hours increased from 58.3 ± 3.1% at pH 7.4 to 82.7 ± 2.8% at pH 5.0. This pH-responsive behavior is a particularly advantageous feature. It can be rationalized by the increased fluidity and potential for structural rearrangement of the lipid bilayer under mildly acidic conditions, alongside the enhanced aqueous solubility of PTX in a slightly acidic medium, which collectively promote more efficient drug diffusion out of the nanoparticle matrix. This differential release profile suggests that the Fe_3O_4-LNP system can provide stable circulation at physiological pH while selectively accelerating drug release within the acidic tumor interstitium or endosomal compartments post-cellular uptake, thereby potentially enhancing therapeutic specificity and reducing systemic side effects.

In Vitro Cytotoxicity Assay

The therapeutic efficacy and biocompatibility of the Fe_3O_4-LNP hybrid system were quantitatively assessed through a comparative cytotoxicity study against two phenotypically distinct breast cancer cell lines: the hormone-responsive MCF-7 and the aggressive, triple-negative MDA-MB-231. The calculated half-maximal inhibitory concentration (IC_{50}) values for all tested formulations after a 48-hour exposure are summarized in Table 3. These values serve as the primary metric for evaluating the potency of the drug delivery system.

The data reveal several critical trends. First, the blank Fe_3O_4-LNP carrier exhibited negligible cytotoxicity, with IC_{50} values exceeding 50 µM (expressed in equivalent nanoparticle concentration), underscoring the inherent biocompatibility of the lipid-coated magnetite hybrid system. This is a fundamental requirement for any delivery vehicle, confirming that observed cytotoxic effects are due to the payload, not the carrier itself. Most notably, the Fe_3O_4-LNP/PTX formulation demonstrated a marked and statistically significant enhancement in cytotoxic potency compared to both free PTX and its commercial Cremophor EL®-based counterpart. Against MCF-7 cells, the IC_{50} of the hybrid nanoparticles (8.6 nM) was approximately 2.1-fold lower than that of free PTX (18.4 nM). This enhancement was even more pronounced in the MDA-MB-231 cell line, where the IC_{50} decreased from 12.7 nM for free drug to 5.9 nM for the nano-formulation a 2.2-fold improvement in potency. This differential effect suggests that the more invasive MDA-MB-231 cells, known for higher endocytic activity, may internalize the nanoparticle formulation more efficiently. The superior performance of Fe_3O_4-LNP/PTX can be attributed to a confluence of factors facilitated by the nano-carrier. The lipid-based encapsulation circumvents the solubility limitations and potential sequestration of free PTX by cellular efflux pumps or serum proteins. More importantly, the nanoparticles are internalized via endocytic pathways, which bypasses passive diffusion and delivers a concentrated bolus of PTX directly into the cytoplasm upon endosomal escape or degradation of the lipid shell. This mechanism effectively increases the intracellular drug concentration at the target site, leading to the observed lower IC_{50} values. The slightly higher IC_{50} of the commercial formulation compared to free PTX likely reflects suboptimal cellular uptake kinetics or minor inhibitory effects of the Cremophor EL® vehicle. Collectively, these results confirm that the Fe_3O_4-LNP hybrid architecture not only successfully delivers PTX but does so with enhanced efficiency, translating to significantly

Table 3. In vitro cytotoxicity (IC_{50}, nM) of various formulations against breast cancer cell lines after 48 h incubation (mean ± SD, n=4).

Formulation	MCF-7 IC_{50} (nM)	MDA-MB-231 IC_{50} (nM)
Free Paclitaxel (PTX)	18.4 ± 2.1	12.7 ± 1.8
Commercial PTX (Cremophor EL®)	21.9 ± 3.0	15.3 ± 2.4
Fe_3O_4-LNP/PTX	8.6 ± 1.2	5.9 ± 0.9
Blank Fe_3O_4-LNP (No Drug)	> 50,000	> 50,000

improved *in vitro* cytotoxicity against both tested breast cancer models.

Cellular Uptake and Localization Studies

The enhanced cytotoxicity of the Fe_3O_4-LNP/PTX formulation logically prompted an investigation into its cellular internalization dynamics, a critical determinant of nanoparticle-mediated drug delivery efficacy. To visualize and quantify uptake, the hybrid nanoparticles were loaded with the lipophilic fluorescent dye DiI, maintaining identical physicochemical properties to the drug-loaded counterparts but allowing for direct tracking.

Qualitative assessment via confocal laser scanning microscopy provided compelling visual evidence of efficient cellular internalization. In MDA-MB-231 cells treated with DiI-labeled Fe_3O_4-LNP, a strong red fluorescence signal was observed predominantly in the perinuclear region after a 4-hour incubation. The signal was punctate and localized within intracellular vesicles, indicative of endocytic uptake pathways. Notably, minimal fluorescence was associated with the cell membrane, confirming that the signal arose from internalized nanoparticles rather than surface adhesion. This intracellular localization pattern is advantageous, as it positions the carrier within the endolysosomal trafficking route, facilitating subsequent drug release into the cytoplasm.

For a quantitative and statistically robust analysis, flow cytometry was employed under identical treatment conditions. The median fluorescence intensity (MFI) of the cell population, normalized to untreated controls, provides a direct measure of nanoparticle association and internalization. The results, summarized in Table 4, offer clear and quantitative support for the microscopy observations.

The data reveal a substantial, 22.8-fold increase in the cellular fluorescence intensity for cells treated with the hybrid nanoparticles compared to the untreated control. This dramatic increase in MFI is a direct quantitative confirmation of extensive and efficient cellular uptake. The relatively low standard deviation across replicates also indicates a consistent and uniform interaction of the nanoparticles with the cell population. The combination of confocal and flow cytometric data provides a comprehensive picture: the Fe_3O_4-LNP hybrids are not only internalized efficiently in bulk, as shown by flow cytometry, but they are also trafficked to relevant intracellular compartments, as visualized by microscopy. This efficient internalization pathway provides a clear mechanistic foundation for the enhanced cytotoxicity observed, as it ensures a greater intracellular concentration of the delivered paclitaxel payload compared to the passive diffusion mechanism of the free drug.

Evaluation of Magnetic Targeting Efficacy

A defining feature of our hybrid design is the potential for spatial guidance via an external magnetic field. To validate this critical functionality, we conducted a proof-of-concept experiment to quantify the magnetic field-enhanced cellular accumulation of the Fe_3O_4-LNP hybrids under controlled *in vitro* conditions. MDA-MB-231 cells were exposed to DiI-labeled nanoparticles in a setup where a magnetic gradient was applied to one half of the culture well, with the other half serving as an internal, non-magnetized control within the same biological replicate. This design minimizes well-to-well variability. After

Table 4. Quantitative cellular uptake of DiI-labeled Fe_3O_4-LNP in MDA-MB-231 cells after 4 h incubation, as determined by flow cytometry (mean ± SD, n=3).

Sample	Median Fluorescence Intensity (MFI)	Fold Increase vs. Control
Untreated Control	1250 ± 180	1.0
DiI-Labeled Fe_3O_4-LNP	28450 ± 2,150	22.8 ± 2.1

Table 5. Magnetic field-enhanced cellular association of DiI-labeled Fe_3O_4-LNP in MDA-MB-231 cells. Data represent median fluorescence intensity (MFI) from flow cytometry for cells from the magnetized and control regions of the same well (mean ± SD, n=4 independent experiments).

Region	Median Fluorescence Intensity (MFI)	Fold Increase (Magnetized/Control)
Control (No Magnet)	15320 ± 1,840	1.0
Magnetized	52470 ± 3,910	3.42 ± 0.31

a 2-hour incubation with gentle agitation to simulate dynamic conditions, cellular association was quantified by flow cytometry. The results, summarized in Table 5, provide unequivocal evidence of magnetically driven targeting.

The data demonstrate a statistically significant and substantial enhancement in nanoparticle association with cells located in the magnetized region. The mean MFI increased from 15,320 in the control region to 52,470 in the region subjected to the magnetic field, corresponding to a 3.4-fold increase in cellular fluorescence. This increase is directly attributable to the magnetic force acting on the superparamagnetic Fe_3O_4 cores, which promotes the directional movement and localized retention of the hybrid nanoparticles at the target cell layer. It is important to note that the control region still exhibits considerable uptake (consistent with the data in Section 3.7), which reflects the inherent, non-targeted cellular internalization of the nanoparticles. The magnetic field does not inhibit this basal process; rather, it superimposes a directional flux that dramatically amplifies local accumulation. This result provides a compelling *in vitro* validation of the core design principle. It confirms that the lipid encapsulation, while essential for stability and drug loading, does not shield the magnetic core's functionality. The demonstrated ability to enhance cellular association by a factor greater than 3 through a simple, externally applied magnetic field underscores the potential of this platform for improving site-specific delivery *in vivo*, where such targeting could help overcome off-target distribution and enhance therapeutic index at the tumor site.

The presented Fe_3O_4-lipid hybrid nanoparticle system successfully demonstrates the synergistic potential of integrating an inorganic magnetic core with an organic lipid bilayer for the enhanced delivery of paclitaxel to breast cancer cells. The synthesis yielded well-defined, superparamagnetic nanostructures with high drug loading, pH-responsive release, significantly improved *in vitro* cytotoxicity, and demonstrable magnetic targeting capability. These results collectively validate our core hypothesis that such a hybrid architecture can address key limitations of conventional chemotherapy, particularly poor solubility and non-specific biodistribution.

However, translating this promising *in vitro* proof-of-concept into a clinically viable therapeutic entails navigating several foreseeable challenges. A primary consideration is the complex interplay between the hybrid nanoparticle's physicochemical properties size, surface charge, lipid composition, and magnetic content and it's *in vivo* pharmacokinetics, including circulation half-life, potential for opsonization, and biodistribution beyond magnetic targeting sites. While our lipid shell is designed for stealth, the long-term stability of the colloidal suspension in biological fluids and the potential for gradual oxidation of the magnetite core require thorough investigation. Furthermore, the efficacy of magnetic targeting *in vivo* is constrained by the depth and strength of the externally applied field, as well as the vascularization and hemodynamics of the tumor microenvironment. Scaling up the synthesis with the requisite batch-to-batch reproducibility for preclinical studies also presents a non-trivial materials engineering challenge.

Future work will therefore be strategically directed towards addressing these translational gaps. Immediate next steps involve comprehensive *in vivo* studies in murine xenograft models to quantify the actual enhancement in tumor accumulation and therapeutic efficacy afforded by magnetic guidance, directly compared to non-targeted administration [47]. Concurrently, we aim to refine the lipid formulation by incorporating PEGylated lipids to further extend circulation time and explore the conjugation of small-molecule targeting ligands (e.g., folic acid) to the lipid surface for active, dual-targeting strategies [48]. From a materials perspective, investigating the coating of the Fe_3O_4 core with a thin silica layer prior to lipid encapsulation could provide enhanced oxidative stability and a more defined interface for functionalization [49]. Ultimately, the goal is to evolve this platform into a multimodal theranostic agent, where the magnetic core could also serve as a contrast agent for magnetic resonance imaging (MRI), enabling real-time monitoring of delivery efficacy. By systematically tackling these challenges, the path can be paved for this hybrid nanocarrier system to progress beyond the bench and towards meaningful oncological applications [50].

CONCLUSION

In this study, we demonstrated the successful synthesis and characterization of Fe_3O_4-lipid hybrid nanoparticles (Fe_3O_4-LNP) as inorganic–organic

nano-carriers for paclitaxel (PTX) delivery in breast cancer models. The Fe_3O_4 core, prepared by a controlled co-precipitation approach, imparted superparamagnetic properties that were retained after lipid encapsulation, enabling potential magnetic guidance and theranostic functionality. The lipid corona, composed of a DSPC-based bilayer with cholesterol stabilization, conferred biocompatibility and provided a versatile matrix for PTX loading. Across three synthesis batches, PTX encapsulation efficiencies approached high values (EE ≈ 85–92%), with a drug loading capacity near 8% (w/w), highlighting the efficiency and reproducibility of the formulation strategy. In vitro release studies revealed a biphasic profile characterized by an initial rapid release followed by a sustained phase, with release kinetics accelerated under acidic conditions (pH ~5.0) that emulate the tumor microenvironment, relative to physiological pH (7.4). This pH-responsive behavior supports preferential PTX delivery at tumor sites while mitigating systemic exposure. Biological evaluation showed enhanced anti-tumor activity of Fe_3O_4-LNP/PTX compared with free PTX and conventional Cremophor EL formulations in breast cancer cell lines, accompanied by improved cellular uptake and magnetically augmented localization. The magnetic responsiveness was evidenced by pronounced accumulation in magnetized regions, suggesting feasibility for image-guided and magnetically targeted therapy. Collectively, Fe_3O_4-LNP/PTX represents a promising inorganic–organic hybrid platform that integrates efficient drug loading, controlled release, biocompatibility, and magnetic guidance, with potential extensions to theranostic applications. Translational challenges stoichiometric optimization, long-term biocompatibility, pharmacokinetics, and in vivo efficacy merit comprehensive in vivo investigations. This work lays a solid foundation for further preclinical studies toward clinical realization of magnetically guided PTX delivery for breast cancer therapy.

CONFLICT OF INTEREST

The authors declare that there is no conflict of interests regarding the publication of this manuscript.

REFERENCES

1. Talluri SV, Kuppusamy G, Karri VVSR, Tummala S, Madhunapantula SV. Lipid-based nanocarriers for breast cancer treatment – comprehensive review. Drug Deliv. 2015;23(4):1291-1305.
2. Sharma A, Jain N, Sareen R. Nanocarriers for Diagnosis and Targeting of Breast Cancer. BioMed Research International. 2013;2013:1-10.
3. Ashrafizadeh M, Zarrabi A, Bigham A, Taheriazam A, Saghari Y, Mirzaei S, et al. (Nano)platforms in breast cancer therapy: Drug/gene delivery, advanced nanocarriers and immunotherapy. Med Res Rev. 2023;43(6):2115-2176.
4. Lao J, Madani J, Puértolas T, Álvarez M, Hernández A, Pazo-Cid R, et al. Liposomal Doxorubicin in the Treatment of Breast Cancer Patients: A Review. Journal of Drug Delivery. 2013;2013:1-12.
5. O'Shaughnessy JA. Pegylated Liposomal Doxorubicin in the Treatment of Breast Cancer. Clin Breast Cancer. 2003;4(5):318-328.
6. Gabizon AA, Gabizon-Peretz S, Modaresahmadi S, La-Beck NM. Thirty years from FDA approval of pegylated liposomal doxorubicin (Doxil/Caelyx): an updated analysis and future perspective. BMJ Oncology. 2025;4(1):e000573.
7. Ghahremanloo A, Erfani B, Asgharzadeh F, Mansoori S, Gheybi F, Hashemy SI. Reducing toxicity and enhancing efficacy of doxorubicin by liposomal doxorubicin and aprepitant in breast cancer. Sci Rep. 2025;15(1).
8. Patel T, Zhou J, Piepmeier JM, Saltzman WM. Polymeric nanoparticles for drug delivery to the central nervous system. Adv Drug Del Rev. 2012;64(7):701-705.
9. Kesharwani P, Jain K, Jain NK. Dendrimer as nanocarrier for drug delivery. Prog Polym Sci. 2014;39(2):268-307.
10. Palmerston Mendes L, Pan J, Torchilin V. Dendrimers as Nanocarriers for Nucleic Acid and Drug Delivery in Cancer Therapy. Molecules. 2017;22(9):1401.
11. Kube S, Hersch N, Naumovska E, Gensch T, Hendriks J, Franzen A, et al. Fusogenic Liposomes as Nanocarriers for the Delivery of Intracellular Proteins. Langmuir. 2017;33(4):1051-1059.
12. Lombardo D, Kiselev MA. Methods of Liposomes Preparation: Formation and Control Factors of Versatile Nanocarriers for Biomedical and Nanomedicine Application. Pharmaceutics. 2022;14(3):543.
13. Unnikrishnan G, Joy A, Megha M, Kolanthai E, Senthilkumar M. Exploration of inorganic nanoparticles for revolutionary drug delivery applications: a critical review. Discover Nano. 2023;18(1).
14. Loh XJ, Lee T-C, Dou Q, Deen GR. Utilising inorganic nanocarriers for gene delivery. Biomaterials Science. 2016;4(1):70-86.
15. Chu M, Shao Y, Peng J, Dai X, Li H, Wu Q, et al. Near-infrared laser light mediated cancer therapy by photothermal effect of Fe_3O_4 magnetic nanoparticles. Biomaterials. 2013;34(16):4078-4088.
16. Fu S, Wang S, Zhang X, Qi A, Liu Z, Yu X, et al. Structural effect of Fe_3O_4 nanoparticles on peroxidase-like activity for cancer therapy. Colloids Surf B Biointerfaces. 2017;154:239-245.
17. S R, M P. Multi-functional core-shell Fe_3O_4@Au nanoparticles for cancer diagnosis and therapy. Colloids Surf B Biointerfaces. 2019;174:252-259.
18. Wang Y, Liu X, Ma S, He X, Guo C, Liang Z, et al. Progress in cancer therapy with functionalized Fe_3O_4 nanomaterials. Frontiers of Materials Science. 2023;17(3).
19. Tian X, Ruan L, Zhou S, Wu L, Cao J, Qi X, et al. Appropriate Size of Fe_3O_4 Nanoparticles for Cancer Therapy by Ferroptosis. ACS Applied Bio Materials. 2022;5(4):1692-1699.

20. Jabir MS, Nayef UM, Abdulkadhim WK, Taqi ZJ, Sulaiman GM, Sahib UI, et al. Fe_3O_4 Nanoparticles Capped with PEG Induce Apoptosis in Breast Cancer AMJ13 Cells Via Mitochondrial Damage and Reduction of NF-κB Translocation. Journal of Inorganic and Organometallic Polymers and Materials. 2020;31(3):1241-1259.
21. Yang H, Li G, Zhang J, Zhao J, Zhao Y, Wu Y, et al. A novel hollow iron nanoparticle system loading PEG-Fe_3O_4 with C5a receptor antagonist for breast cancer treatment. Front Immunol. 2024;15.
22. Adimoolam MG, Amreddy N, Nalam MR, Sunkara MV. A simple approach to design chitosan functionalized Fe_3O_4 nanoparticles for pH responsive delivery of doxorubicin for cancer therapy. J Magn Magn Mater. 2018;448:199-207.
23. Li J, Zhang W, Gao Y, Tong H, Chen Z, Shi J, et al. Near-infrared light and magnetic field dual-responsive porous silicon-based nanocarriers to overcome multidrug resistance in breast cancer cells with enhanced efficiency. Journal of Materials Chemistry B. 2020;8(3):546-557.
24. Kang X, Sun T, Zhang L, Zhou C, Xu Z, Du M, et al. Synergistic Theranostics of Magnetic Resonance Imaging and Photothermal Therapy of Breast Cancer Based on the Janus Nanostructures Fe_3O_4-Aushell-PEG. International Journal of Nanomedicine. 2021;Volume 16:6383-6394.
25. Borji S, Shahriarinour M, Shariati S, Ranji N, Nikpassand M. Enhanced therapeutic efficacy of silibinin loaded silica coated magnetic nanocomposites against Pseudomonas aeruginosa in Combination with Ciprofloxacin and HepG2 cancer cells. Sci Rep. 2025;15(1).
26. Lai X, Zhao Y, Shi Z, Xing L, Li X, Jia L, et al. Plant-derived paclitaxel-loaded ultra-small Fe_3O_4 nanoparticles for MR imaging-mediated antitumor therapy. Industrial Crops and Products. 2025;228:120902.
27. Tavakoli M, Maghsoudian S, Rezaei-Aderiani A, Hajiramezanali M, Fatahi Y, Amani M, et al. Synergistic effects of paclitaxel and platelet-superparamagnetic iron oxide nanoparticles for targeted chemo-hyperthermia therapy against breast cancer. Colloids Surf B Biointerfaces. 2025;251:114584.
28. Siontorou C, Nikoleli G-P, Nikolelis D, Karapetis S. Artificial Lipid Membranes: Past, Present, and Future. Membranes. 2017;7(3):38.
29. Zardavas D, Irrthum A, Swanton C, Piccart M. Clinical management of breast cancer heterogeneity. Nature Reviews Clinical Oncology. 2015;12(7):381-394.
30. Patani N, Martin LA, Dowsett M. Biomarkers for the clinical management of breast cancer: International perspective. Int J Cancer. 2013;133(1):1-13.
31. Jafari N, Mohammadpourfard M, Hamishehkar H. A comprehensive study on doxorubicin-loaded aspartic acid-coated magnetic Fe_3O_4 nanoparticles: Synthesis, characterization and in vitro anticancer investigations. J Drug Deliv Sci Technol. 2024;100:106133.
32. Go YK, Leal C. Polymer–Lipid Hybrid Materials. Chem Rev. 2021;121(22):13996-14030.
33. Rahamathulla M, Bindiya R, Venkatesh MP, Pai DR, Harshith HS, Ghazwani M, et al. Design and optimization of intranasal aripiprazole-loaded nanostructured lipid carriers for enhanced brain targeting in schizophrenia: in vitro and ex vivo evaluation. Sci Rep. 2025;15(1).
34. Niles AL, Moravec RA, Riss TL. Update on in vitro cytotoxicity assays for drug development. Expert Opinion on Drug Discovery. 2008;3(6):655-669.
35. Matczuk M, Ruzik L, Aleksenko SS, Keppler BK, Jarosz M, Timerbaev AR. Analytical methodology for studying cellular uptake, processing and localization of gold nanoparticles. Anal Chim Acta. 2019;1052:1-9.
36. Cao Q, Han X, Li L. Enhancement of the efficiency of magnetic targeting for drug delivery: Development and evaluation of magnet system. J Magn Magn Mater. 2011;323(15):1919-1924.
37. Chen J, Wang F, Huang K, Liu Y, Liu S. Preparation of Fe_3O_4 nanoparticles with adjustable morphology. J Alloys Compd. 2009;475(1-2):898-902.
38. Qu J, Liu G, Wang Y, Hong R. Preparation of Fe3O4–chitosan nanoparticles used for hyperthermia. Adv Powder Technol. 2010;21(4):461-467.
39. Hong R, Li J, Wang J, Li H. Comparison of schemes for preparing magnetic Fe_3O_4 nanoparticles. China Particuology. 2007;5(1-2):186-191.
40. Shen YF, Tang J, Nie ZH, Wang YD, Ren Y, Zuo L. Preparation and application of magnetic Fe3O4 nanoparticles for wastewater purification. Sep Purif Technol. 2009;68(3):312-319.
41. Dehghani-Ghahnaviyeh S, Smith M, Xia Y, Dousis A, Grossfield A, Sur S. Ionizable Amino Lipids Distribution and Effects on DSPC/Cholesterol Membranes: Implications for Lipid Nanoparticle Structure. The Journal of Physical Chemistry B. 2023;127(31):6928-6939.
42. Wei Y, Han B, Hu X, Lin Y, Wang X, Deng X. Synthesis of Fe_3O_4 Nanoparticles and their Magnetic Properties. Procedia Engineering. 2012;27:632-637.
43. Abutalib MM, Rajeh A. Influence of Fe_3O_4 nanoparticles on the optical, magnetic and electrical properties of PMMA/PEO composites: Combined FT-IR/DFT for electrochemical applications. J Organomet Chem. 2020;920:121348.
44. Silva VAJ, Andrade PL, Silva MPC, Bustamante D A, De Los Santos Valladares L, Albino Aguiar J. Synthesis and characterization of Fe_3O_4 nanoparticles coated with fucan polysaccharides. J Magn Magn Mater. 2013;343:138-143.
45. Liang J, Yang X, Liu D, Cong M, Song Y, Bai S. Lipid/Hyaluronic Acid–Coated Doxorubicin-Fe_3O_4 as a Dual-Targeting Nanoparticle for Enhanced Cancer Therapy. AAPS PharmSciTech. 2020;21(6).
46. Kilic A, Emin Karatas M, Beyazsakal L, Okumus V. Preparation and spectral studies of boronate ester modified magnetite iron nanoparticles (Fe_3O_4@APTES-B) as a new type of biological agents. J Mol Liq. 2022;361:119602.
47. Shen L, Li B, Qiao Y. Fe_3O_4 Nanoparticles in Targeted Drug/Gene Delivery Systems. Materials. 2018;11(2):324.
48. Nordin A, Ahmad Z, Husna S, Ilyas R, Azemi A, Ismail N, et al. The State of the Art of Natural Polymer Functionalized Fe_3O_4 Magnetic Nanoparticle Composites for Drug Delivery Applications: A Review. Gels. 2023;9(2):121.
49. Vallabani NVS, Singh S. Recent advances and future prospects of iron oxide nanoparticles in biomedicine and diagnostics. 3 Biotech. 2018;8(6).
50. Wang X, Zhang R, Wu C, Dai Y, Song M, Gutmann S, et al. The application of Fe_3O_4 nanoparticles in cancer research: A new strategy to inhibit drug resistance. Journal of Biomedical Materials Research Part A. 2006;80A(4):852-860.